Effect of Adhesion Geometry and Rigidity on Cellular Force Distributions

Ilka B. Bischofs,[1,2,*] Sebastian S. Schmidt,[1,3] and Ulrich S. Schwarz[1,4,†]

[1]*Bioquant, University of Heidelberg, Im Neuenheimer Feld 267, 69120 Heidelberg, Germany*
[2]*Physical Biosciences Division, Lawrence Berkeley National Lab, Berkeley, California 94710, USA*
[3]*Helmholtz-Zentrum Berlin, Glienicker Strasse 100, 14109 Berlin, Germany*
[4]*Theoretical Biophysics Group, University of Karlsruhe, 76128 Karlsruhe, Germany*

(Received 10 February 2009; published 23 July 2009)

The behavior and fate of tissue cells are controlled by the rigidity and geometry of their adhesive environment, possibly through forces localized to sites of adhesion. We introduce a mechanical model that predicts cellular force distributions for cells adhering to adhesive patterns with different geometries and rigidities. For continuous adhesion along a closed contour, forces are predicted to be localized to the corners. For discrete sites of adhesion, the model predicts the forces to be mainly determined by the lateral pull of the cell contour. With increasing distance between two neighboring sites of adhesion, the adhesion force increases because the cell shape results in steeper pulling directions. Softer substrates result in smaller forces. Our predictions agree well with experimental force patterns measured on pillar assays.

DOI: 10.1103/PhysRevLett.103.048101 PACS numbers: 87.10.−e, 68.03.Cd, 87.17.Rt

Adherent tissue cells react very sensitively to the physical properties of their environment, including mechanical stiffness and the spatial distribution of adhesive cues [1]. On flat substrates, mechanical stiffness and adhesive geometry can be controlled by using soft elastic substrates [2] and microcontact printing of adhesive islands [3], respectively. Rigidity and geometry can be altered simultaneously combining the above techniques [4,5] or by using biofunctionalized pillar assays, in which cells adhere to the tops of an array of flexible microneedles [6,7]. Such biophysical approaches have revealed that stiffness and geometry sensing are closely related as they both involve forces being localized at discrete adhesion sites.

Despite the tremendous experimental progress in this field, our theoretical understanding of the relation among stiffness sensing, geometry sensing, and cellular force distributions is still very limited. Here we analyze a simple theoretical model that describes the relation between cell shape and force distribution. The shape of tissue cells adhering to discrete sites of adhesion is dominated by the formation of inward curved circular arcs of the nonadherent contour [8–11]. This shape feature follows from a modified Laplace law of competing effective surface tension and effective line tension. Based on these concepts, we calculate traction forces of stationary cells as a function of adhesive geometry and stiffness.

Model.—Fully spread tissue cells typically flatten with only the nucleus sticking out, as shown schematically in Fig. 1(a). Often they adhere to the substrate at sites of adhesion distributed along the cell boundary. In this case, it is appropriate to consider an effectively two-dimensional (2D) model which parametrizes cell shape by its 2D contour $\vec{r}(l)$ with the internal coordinate l. After cell spreading is completed, the cellular forces are mainly contractile. Figure 1(b) depicts the physical forces acting at the cell boundary [8]. First, the cell contour is drawn inward mainly due to spatially distributed tension in the actin cytoskeleton and the plasma membrane. In the 2D model, this effect is described by an effective surface tension σ, because the main effect is to reduce 2D surface area. Second, the cell contour resists the inward pull. Often the cell contour is reinforced by the assembly of contractile actin cables connecting neighboring sites of adhesion. In the 2D model, this effect is described by an effective line tension λ which contracts the contour between adhesion sites. In mechanical equilibrium, the contractile forces

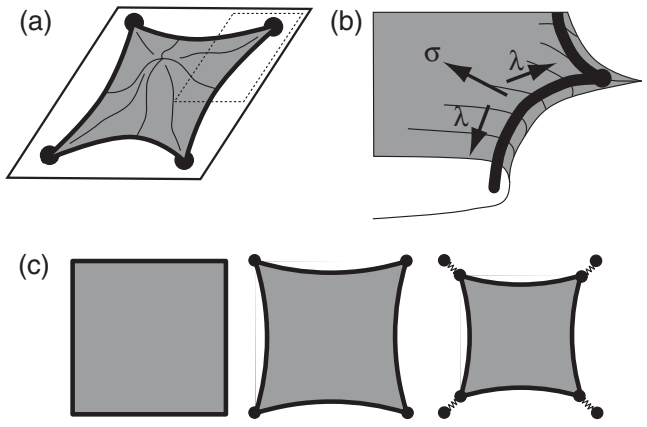

FIG. 1. (a) Cartoon of a typical tissue cell adhering to a flat substrate at four discrete sites of adhesion. In (b) we focus on the framed region. (b) Physical forces acting at the free boundary between two neighboring sites of adhesion: While the surface tension σ pulls the contour inward, the line tension λ pulls the contour straight. The black line represents an actin cable reinforcing the contour. (c) Here we consider three cases of increasing complexity: cells adhering to one large adhesive island, cells adhering to discrete sites of adhesion on a rigid substrate, and cells adhering to discrete sites of adhesion on a soft substrate.

exerted by cells are primarily balanced on the adhesive substrate [12]. To derive the force distribution for a given adhesive geometry, we therefore have to minimize the effective energy functional for the cell contour under the appropriate adhesion constraint:

$$E = \int \sigma dA + \int \lambda dl + \int \vec{f}_{\mathrm{ad}} \cdot (\vec{r} - \vec{r}_0) dl. \qquad (1)$$

The first integral extends over the cell surface area A and the second and third along the cell contour l. The third term introduces the adhesion tension $\vec{f}_{\mathrm{ad}}$ as a Lagrangian parameter for the constraint set by the adhesion geometry and described by $\vec{r}_0$. Based on this model, we calculate the cellular adhesion forces by solving the corresponding Euler-Lagrange equation for the three cases depicted in Fig. 1(c).

Continuous adhesion.—For cells that adhere continuously to the substrate, the cellular shape $\vec{r}$ is fixed to $\vec{r}_0$. The adhesion tension acting along the contour then follows from Eq. (1):

$$\vec{f}_{\mathrm{ad}} = -[\sigma + \lambda\kappa]\vec{n}, \qquad (2)$$

where $\vec{n}$ is the normal vector of the contour curve and κ its local curvature. For convex shapes ($\kappa > 0$), surface and line tension conspire to pull the cell contour inward, while for concave shapes ($\kappa < 0$), the line tension opposes the surface tension, thereby decreasing the adhesion force. For example, a cell adhering to a circular patch of radius R applies a constant and inwardly directed adhesive tension $\sigma + \lambda/R$ along the contour. Along straight boundaries ($\kappa = 0$), e.g., along the straight lines of polygonal cells, the contribution of the line tension λ vanishes and the adhesion tension is simply σ. The contribution of the line tension localizes to the corners of the polygon. Approximating a corner with opening angle ϕ by an arc with radius ϵ and then taking the limit to a sharp corner by $\epsilon \to 0$, we can calculate the adhesion force $\vec{F}$ acting in the corner:

$$\vec{F} = \lim_{\epsilon \to 0} \int_{-\frac{\varphi}{2}}^{\frac{\varphi}{2}} \left(\sigma + \frac{\lambda}{\epsilon}\right) \vec{n}(\theta) \epsilon d\theta = 2\lambda \cos\left(\frac{\phi}{2}\right) \vec{n}_b, \qquad (3)$$

where $\varphi = \pi - \phi$ and $\vec{n}_b$ points in the direction of the bisecting line. The model predicts that the smaller ϕ, the larger the force pulling on the corner, with a maximal value of 2λ when both arcs pull in the same direction. When considering a finite radius r of the adhesion, one has to set $\epsilon = r$ rather than taking the limit $\epsilon \to 0$, resulting in an additional contribution by the surface tension σ. Experimentally, cells have been forced into various shapes and forces have been measured by using adhesive islands on compliant substrates [4]. On polygonal islands, strong traction forces are measured at the corners. Our model qualitatively predicts this corner effect and makes quantitative predictions on the scaling with ϕ which can be experimentally tested in the future.

Discrete adhesion.—For cells that adhere to the substrate at discrete points of adhesion, the cell contour between adhesion points is free, and the shape equation resulting from Eq. (1) predicts the formation of circular arcs with curvature $\kappa = \sigma/\lambda$. The adhesion force follows from Eq. (3) by replacing the opening angle ϕ with the actual pulling angle $\phi^\star \neq \phi$ spanned by the two contour arcs pulling on the adhesion site. $\phi^\star$ has to be derived from the shape equation. For three equally spaced adhesion sites with distance d spanning an angle ϕ, we can derive an explicit equation for the resultant force on the central adhesion site as a function of the adhesion geometry:

$$\vec{F} = 2\lambda\left[\beta \sin\left(\frac{\phi}{2}\right) + \sqrt{1 - \beta^2}\cos\left(\frac{\phi}{2}\right)\right]\vec{n}_b, \qquad (4)$$

with $\beta = \sigma d/2\lambda$ being a dimensionless measure for the strength of the inward pull. β can also be interpreted as dimensionless spanning distance d. Hence, the force scales again with the line tension λ but now also depends on the spanning distance d and the surface tension σ. Figure 2(a) demonstrates that the larger the spanning distance d and the more acute the opening angle ϕ, the steeper the inward

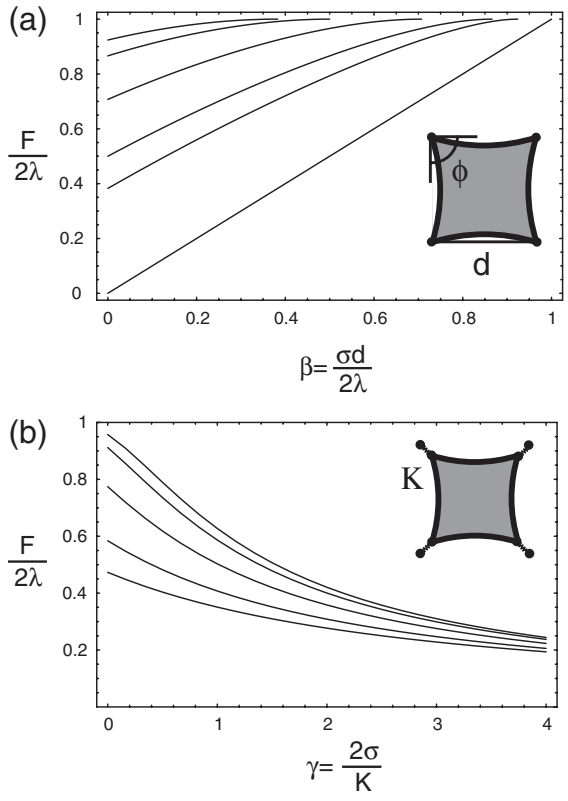

FIG. 2. (a) Dimensionless force $F/2\lambda$ at equally spaced adhesion points as a function of the dimensionless spanning distance $\beta = \sigma d/2\lambda$ for different opening angles $\phi = \pi/4$, $\pi/3$, $\pi/2$, $2\pi/3$, $3\pi/4$, and π from top to bottom. (b) Dimensionless force $F/2\lambda$ as a function of the dimensionless inverse stiffness $\gamma = 2\sigma/K$ for adhesion to regular polygons with $\phi = \pi/4$, $\pi/3$, $\pi/2$, $2\pi/3$, and $3\pi/4$ from top to bottom and $\beta = 0.1$.

pull and the closer the force comes to its maximal value 2λ. This maximal value is reached at a critical pulling strength $\beta_c = \sin(\phi/2)$ when the pulling direction has become so steep that the two arcs physically touch each other ($\phi^\star = 0$), at which point other physical processes will take over (e.g., pearling of tubular extensions [9]). For equally spaced adhesion sites along a straight line $\phi = \pi$, the adhesion force scales exactly linear with spanning distance d. As the opening angle ϕ increases beyond π, the traction force may become a pushing force. For unequal spacing $d_1 \neq d_2$ between adhesion sites, a generalization of Eq. (4) can be derived, which shows that the force direction is now tilted towards the side with the larger spanning distance.

Elastic substrate.—To study how in our model elasticity affects the adhesion force, we now consider discrete adhesion sites that move in a harmonic potential with spring constant K. For simplicity, we consider only regular polygons, for which we find

$$\vec{F} = 2\lambda\left[\frac{\beta\gamma_\phi + \cos(\frac{\phi}{2})\sqrt{\gamma_\phi^2 + \cos^2(\frac{\phi}{2}) - \beta^2}}{\gamma_\phi^2 + \cos^2(\frac{\phi}{2})}\right]\vec{n}_b, \quad (5)$$

with $\gamma_\phi = \sin(\phi/2) + \gamma\cos(\phi/2)$. Here $\gamma = 2\sigma/K$ is a dimensionless inverse stiffness. Figure 2(b) shows that the maximal adhesion force is reached on a rigid substrate $\gamma = 0$, where Eq. (5) reduces to Eq. (4). As the substrate becomes softer, F decreases because the moving adhesion points effectively decrease the spanning distance d. Indeed, it is well known that cellular traction is weaker on softer substrates [2]. Like for rigid substrates, the force decreases with increasing opening angle. Both of these trends are also evident in Figs. 3(a)–3(c), where we show computed cell shapes for triangles, squares, and pentagons on stiff (red) and elastic (blue) substrates.

Tension-elasticity model.—Up to now, our results were derived with the assumption of constant line tension λ. Recently, it was suggested that this quantity has an elastic origin, i.e., $\lambda = EAu$, where $u = (L - L_0)/L_0$ is the strain induced in the elastic contour with rigidity EA. $L_0 = \alpha d$ is the resting length assumed to be proportional to the spanning distance d with a dimensionless resting length parameter α. The arc contour length follows from geometrical considerations as $L = 2R\arcsin(d/2R)$, where R is the arc radius. Hence, the line tension λ itself becomes a function of the adhesion geometry:

$$\lambda(d) = EA\left[\frac{2R}{\alpha d}\arcsin\left(\frac{d}{2R}\right) - 1\right], \quad (6)$$

which increases with d. Thus also the radius of curvature $R = \lambda(d)/\sigma$ increases with d, as indeed observed experimentally [11]. The distance dependence of the adhesion force now becomes a nontrivial function of the adhesion distance d. On the one hand, the line tension increases with d, thereby increasing the individual forces pulling on the adhesions. On the other hand, the arc curvature $\kappa = \sigma/\lambda(d)$ decreases with increasing d, leading to less steep pulling directions and therefore reduced overall force. In Fig. 3(d), we compare the results of the tension-elasticity model (green) to the constant tension model (red), where all arcs have the same curvature $\kappa = \sigma/\lambda$. For the tension-elasticity model, the two top arcs across the diagonal have a reduced curvature κ, because here the spanning distance d is increased by a factor of $\sqrt{2}$. The total force magnitude slightly decreases due to less steep pulling directions, although the tension in the individual arcs actually increases.

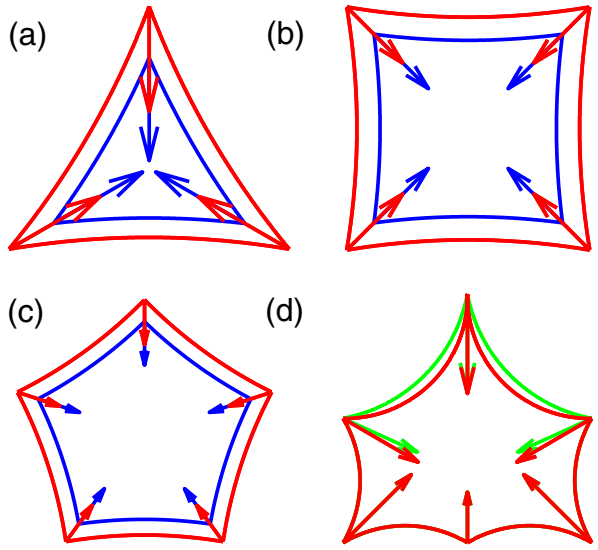

FIG. 3 (color online). (a)–(c) Predicted cell shapes and adhesion forces for various adhesion geometries on stiff $\gamma = 0$ (red) and compliant substrates $\gamma = 1/15$ (blue). Parameters $\beta = 1/6$ and $\phi = \pi/3$, $\pi/2$, and $3/5\pi$ from (a) to (c). (d) Predicted cell shape and adhesion forces on a rigid substrate using constant line tension (red) and the tension-elasticity model (green, $\alpha = 1$, $l_f = 20a$) for an adhesion geometry with different spanning distances, namely, $d = a$ at the sides and $d = \sqrt{2}a$ at the top. In the constant tension model, λ was adjusted to result in the same force for $d = a$.

Extracting model parameters from pillar assays.—In general, one expects the surface tension σ to be a global quantity and the line tensions λ to be different in different arcs. Our model suggests a simple procedure to estimate numerical values from the shape geometry. Figure 4(a) shows experimental data for an endothelial cell on a pillar array (Fig. 6 from Ref. [6]). The contour was fitted by circular arcs using the procedure from Ref. [11]. Because here we focus on contour effects, we exclude all arcs which might interact with other arcs due to close proximity or which might be distorted by internal stress fibers. The force on a pillar is the vector sum of the two adjacent arc forces. Assuming constant surface tension, the ratio of arc radii equals the ratio of line tensions $R_1/R_2 = \lambda_1/\lambda_2$, and the respective pulling angles β_i are given by $\cos\beta_i = R_i/2d_i$. Thus, the resultant *directions* of the contour forces $\vec{F}$ are

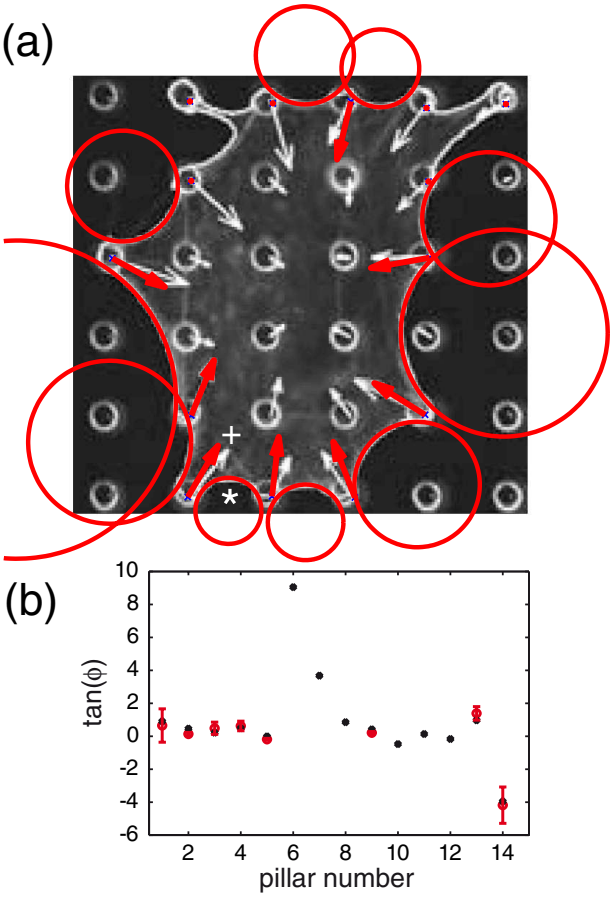

FIG. 4 (color online). (a) Predicted contour forces (red) and measured pillar forces (white) for an endothelial cell cultured on a pillar array [6]. Force direction is determined by cell shape geometry and force magnitude scales with σ as determined from a least-squares fit. Our procedure allows us to predict the forces within each arc $\lambda = (8, 9, 15, 25, 16, 9, 12, 13, 38, 19)$ nN along the contour (counterclockwise starting at the asterisk). Scales: Pillar spacing 9 μm; force with plus 14 nN. (b) Force directions of pillar forces (black) and predicted contour forces (red).

determined by R and d only. Figure 4(b) shows that we obtain excellent agreement between the predicted directions of contour forces and the measured directions of the pillar forces (error bars result from an estimated 10% uncertainty). Because the surface tension determines the *magnitudes* of the contour forces, we extract a value of $\sigma \approx 2$ nN/μm by a least-squares fit to the experimental data, which is at the upper limit of the range of values reported earlier for cortical tension. The predicted contour forces (red) are shown in Fig. 4(a) and compare favorably with the measured pillar forces (white).

Discussion.—Our model shows that shape and forces are closely related in cell adhesion and demonstrates how the spatial distribution of adhesion sites determines the forces acting at sites of adhesion. The effect of these forces might be further amplified by feeding into force or displacement-dependent regulation of cytoskeleton and adhesion sites, which should be included in future modeling. For example, Eq. (5) predicts that displacement F/K first increases linearly and then saturates as a function of inverse stiffness K, with important consequences for strain homeostasis. In this way, our model can be used to derive quantitative predictions how cell behavior and fate can be steered by adhesion geometry and stiffness.

We thank Franziska Klein, Dirk Lehnert, and Martin Bastmeyer for many helpful discussions and Chris Chen and Chris Lemmon for providing supplementary data for Fig. 4. This work was supported by the Center for Modelling and Simulations in the Biosciences (BIOMS) at Heidelberg and by the Karlsruhe Institute of Technology (KIT) through its Concept for the Future.

*ilka@bischofs-pfeifer.eu
†Ulrich.Schwarz@kit.edu

[1] B. Geiger, J. P. Spatz, and A. Bershadsky, Nat. Rev. Mol. Cell Biol. **10**, 21 (2009).
[2] R. J. Pelham and Y.-L. Wang, Proc. Natl. Acad. Sci. U.S.A. **94**, 13 661 (1997).
[3] C. S. Chen, M. Mrksich, S. Huang, G. W. Whitesides, and D. E. Ingber, Science **276**, 1425 (1997).
[4] N. Wang, E. Ostuni, G. W. Whitesides, and D. E. Ingber, Cell Motil. Cytoskeleton **52**, 97 (2002).
[5] J. M. Goffin, P. Pittet, G. Csucs, J. Lussi, J. J. Meister, and B. Hinz, J. Cell Biol. **172**, 259 (2006).
[6] C. A. Lemmon, N. J. Sniadecki, S. A. Ruiz, J. L. Tan, L. H. Romer, and C. S. Chen, Mech. Chem. Biosyst. **2**, 1 (2005).
[7] A. Saez, M. Ghibaudo, A. Buguin, P. Silberzan, and B. Ladoux, Proc. Natl. Acad. Sci. U.S.A. **104**, 8281 (2007).
[8] M. S. Zand and G. Albrecht-Buehler, Cell Motil. Cytoskeleton **13**, 195 (1989).
[9] R. Bar-Ziv, T. Tlusty, E. Moses, S. A. Safran, and A. Bershadsky, Proc. Natl. Acad. Sci. U.S.A. **96**, 10 140 (1999).
[10] M. Thery, A. Pepin, E. Dressaire, Y. Chen, and M. Bornens, Cell Motil. Cytoskeleton **63**, 341 (2006).
[11] I. B. Bischofs, F. Klein, D. Lehnert, M. Bastmeyer, and U. S. Schwarz, Biophys. J. **95**, 3488 (2008).
[12] N. Wang, K. Naruse, D. Stamenovic, J. Fredberg, S. Mijailovich, I. Tolic-Norrelykke, T. Polte, R. Mannix, and D. Ingber, Proc. Natl. Acad. Sci. U.S.A. **98**, 7765 (2001).